

Exchange-correlation potentials for multi-orbital quantum dots subject to generic density-density interactions and Hund's rule coupling

Nahual Sobrino,^{1,2} Stefan Kurth,^{2,3,1} and David Jacob^{2,3,*}

¹*Donostia International Physics Center (DIPC),*

Paseo Manuel de Lardizabal 4, E-20018 San Sebastián, Spain

²*Nano-Bio Spectroscopy Group and European Theoretical Spectroscopy Facility (ETSF),*

Dpto. de Física de Materiales, Universidad del País Vasco UPV/EHU, Av. Tolosa 72, E-20018 San Sebastián, Spain

³*IKERBASQUE, Basque Foundation for Science, Maria Diaz de Haro 3, E-48013 Bilbao, Spain*

(Dated: February 19, 2020)

By reverse-engineering from exact solutions we obtain Hartree-exchange-correlation (Hxc) potentials for a double quantum dot subject to generic density-density interactions and Hund's rule coupling. We find ubiquitous step structures of the Hxc potentials that can be understood and derived from an analysis of stability diagrams. We further show that a generic Hxc potential can be decomposed into four basic potentials which allows for a straight-forward parametrization and paves the road for the construction of Hxc potentials for interacting multi-orbital systems. Finally we employ our parametrization of the Hxc potential in density functional theory calculations of multi-orbital quantum dots and find excellent agreement with exact many-body calculations.

I. INTRODUCTION

Density functional theory (DFT) is one of the most successful and popular approaches for computing the electronic structure of molecules and solids.¹⁻³ Its success is largely owed to its relative simplicity as well as its low computational cost as compared to other quantum many-body approaches. While DFT is in principle exact theory for computing the ground state energy and density of a many-electron system, in practice approximations have to be made to the exchange-correlation (xc) part of the total energy functional. The most popular approximations are the local density (LDA)² and generalized gradient approximations (GGA)⁴⁻⁷ in condensed matter physics, and the so-called hybrid functionals in chemistry.^{8,9} While these approximations usually work quite well for systems with weak to moderate electronic interactions, they completely fail for so-called strongly correlated systems where the interactions between electrons dominate over the kinetic energy. Since DFT is a formally exact theory which is valid also in the strongly correlated regime, this failure has to be assigned to shortcomings of the approximations used. Apparently, the crucial ingredient missing in standard functionals is the so-called derivative discontinuity,¹⁰ i.e., the discontinuous jump of the exact xc potential of an open system as the particle number crosses an integer.^{11,12} In strongly correlated systems the derivative discontinuity contributes a substantial part, e.g., to the fundamental gap or plays a crucial role in the binding and dissociation of molecules.

The essential physics of strongly correlated systems can already be captured by simple but highly nontrivial lattice models such as the Anderson¹³ or the Hubbard model¹⁴ which can be solved by advanced many-body methods as for example Dynamical Mean-Field Theory (DMFT).¹⁵ One way around the problems of the standard approximations of DFT is then to combine DFT with advanced many-body calculations of lattice models.

In these approaches the model Hamiltonian describes the strongly interacting part of the system, while the weakly to moderately interacting part is still described at the level of DFT. An important example is the combination of DFT with DMFT (DFT+DMFT).¹⁶ Originally established for the description of bulk materials, more recently the DFT+DMFT approach has been applied to the description of nanoscale systems¹⁷ and molecules¹⁸. However, this approach is hampered by the so-called double-counting problem¹⁹, limiting its predictivity. More recently, however, new efforts in combining DFT with lattice models avoiding the double-counting problem²⁰⁻²² or to solve the double-counting problem in DFT+DMFT²³ have been undertaken.

Lattice models can also be solved by a lattice version of DFT, an idea which has been pioneered by Schönhammer.^{24,25} Later this approach has been further extended to study lattice problems not only in equilibrium²⁶⁻³⁴ but also in out-of-equilibrium situations such as external time-dependent driving fields³⁵⁻⁴¹ or (steady-state) transport⁴²⁻⁴⁴. A common theme in many of these studies is again the crucial role of the derivative discontinuity (or, alternatively, step features in the xc potential) in the correct description of strongly correlated systems. For instance, for the Hubbard model the derivative discontinuity is the only contribution to the band gap, i.e. the mechanism responsible for opening the Mott-Hubbard gap within DFT.²⁶

Here, in the same framework of lattice DFT, we aim for a better understanding of the structure of the (equilibrium) xc potentials of small lattice models. To this end we extensively study a double quantum dot (DQD) subject to generic interactions as the simplest possible model system for a strongly correlated multi-orbital system. Using reverse-engineering, we construct the exact xc potentials whose essential features are step structures which depend on the particular choice of the interaction. We illustrate how these step structures can be inferred from an analysis of the stability diagram, i.e., regions

of different ground states in the parameter space given by the single-particle level structure. Analysis of the reverse-engineered xc potentials reveals that they can be constructed from four basic building blocks which can be rationalized by a corresponding decomposition of the electron-electron interaction. It is exactly this decomposition of the interaction and the corresponding xc potentials which then allows us to build xc functionals for multi-orbital quantum dots with more than two orbitals.

II. MODEL

We consider a multi-orbital quantum dot (QD) with \mathcal{M} orbitals subject to direct Coulomb repulsion and Hund's rule coupling. The corresponding Hamiltonian reads:

$$\begin{aligned} \mathcal{H} = & \sum_{\alpha} v_{\alpha} \hat{n}_{\alpha} + \sum_{\alpha} U_{\alpha} \hat{n}_{\alpha\uparrow} \hat{n}_{\alpha\downarrow} + \sum_{\alpha < \beta} U_{\alpha\beta} \hat{n}_{\alpha} \hat{n}_{\beta} \\ & - \sum_{\alpha < \beta, \sigma} J_{\alpha\beta} \left[\hat{n}_{\alpha\sigma} \hat{n}_{\beta\sigma} + \left(c_{\alpha\sigma}^{\dagger} c_{\alpha\bar{\sigma}} c_{\beta\bar{\sigma}}^{\dagger} c_{\beta\sigma} \right) \right] \quad (1) \end{aligned}$$

where $c_{\alpha\sigma}$ ($c_{\alpha\sigma}^{\dagger}$) are the annihilation (creation) operators for orbital α and spin σ , $\hat{n}_{\alpha\sigma}$ is the corresponding number operator and $\hat{n}_{\alpha} = \hat{n}_{\alpha\uparrow} + \hat{n}_{\alpha\downarrow}$. U_{α} is the direct intra-orbital Coulomb repulsion for orbital α , $U_{\alpha} \equiv \langle \alpha, \alpha | \hat{V}_c | \alpha, \alpha \rangle$, and $U_{\alpha\beta}$ is the direct inter-orbital Coulomb repulsion between electrons in two different orbitals, $U_{\alpha\beta} = \langle \alpha, \beta | \hat{V}_c | \alpha, \beta \rangle$ for $\alpha \neq \beta$. $J_{\alpha\beta}$ is the Hund's rule coupling, i.e. the exchange integral of the Coulomb interaction, $J_{\alpha\beta} = \langle \alpha, \beta | \hat{V}_c | \beta, \alpha \rangle$ for $\alpha \neq \beta$. Note that here we have split already the Hund's rule term into the density-density contribution (first term in the last line) and the spin-flip contribution (last term). v_{α} are the on-site energies (single-particle energies) of the orbitals α which can be tuned by an external "gate" potential. From here on we will thus refer to v_{α} as the gate potential or simply gate for orbital α .

Here we work at (typically small) finite temperature T and consider the grand canonical ensemble (GCE). The corresponding density matrix (statistical operator) is thus given by

$$\hat{\Gamma} = \frac{e^{-\beta\mathcal{H}}}{Z} = \frac{1}{Z} \sum_m e^{-\beta E_m} |m\rangle \langle m| \quad (2)$$

where $\beta = 1/T$ and Z is the GCE partition function with the chemical potential μ set to zero for convenience. The $|m\rangle$ are the many-body eigenstates of the QD and E_m the corresponding eigenenergies, i.e. $\mathcal{H} |m\rangle = E_m |m\rangle$. Note that the many-body eigenstates $|m\rangle$ are simply Slater determinants here built from the single particle orbitals $|\phi_{\alpha\sigma}\rangle = c_{\alpha\sigma}^{\dagger} |0\rangle$ where $|0\rangle$ is the vacuum state.

III. REVERSE-ENGINEERING OF HXC POTENTIALS AT FINITE TEMPERATURE

In our truncated Hilbert space the density is uniquely defined by the occupancies $\{n_{\alpha}\}$ of the QD orbitals. The Mermin theorem⁴⁵ (the finite-temperature version of the Hohenberg-Kohn theorem¹) then establishes a one-to-one correspondence between the density (occupancies) and the external potential (gate): $\{n_{\alpha}\} \xleftrightarrow{1-1} \{v_{\alpha}\}$ or, in other words, the external potential is a functional of the occupancies, i.e., $v_{\alpha} = v_{\alpha}[\{n_{\alpha'}\}]$.

In order to proceed we introduce the Kohn-Sham (KS) system i.e. an effective non-interacting system that exactly reproduces the density $\{n_{\alpha}\}$ of the many-body Hamiltonian \mathcal{H} .² Here the KS Hamiltonian is already diagonal in the original single-particle basis, i.e.,

$$\mathcal{H}^s = \sum_{\alpha} v_{\alpha}^s \hat{n}_{\alpha}. \quad (3)$$

and the KS orbitals are identical to the original basis orbitals $|\phi_{\alpha\sigma}^s\rangle \equiv |\phi_{\alpha\sigma}\rangle$ with their eigenenergies given by the KS (gate) potentials v_{α}^s . The Hartree-exchange-correlation (Hxc) potentials v_{α}^{Hxc} are defined as the difference between the KS gate and the actual gate potential:

$$v_{\alpha}^{\text{Hxc}}[\{n_{\alpha'}\}] = v_{\alpha}^s[\{n_{\alpha'}\}] - v_{\alpha}[\{n_{\alpha'}\}]. \quad (4)$$

The Hxc potential depends on the electron density which is completely determined by the occupancies of the QD orbitals $\{n_{\alpha}\}$.

In order to determine the Hxc potential \hat{v}_{Hxc} as a functional of the density $\{n_{\alpha}\}$, the many-body problem given by \mathcal{H} is solved for a given set of gates $\{v_{\alpha}\}$. The resulting set of eigenstates and corresponding energies determines the density in the GCE according to:

$$n_{\alpha} = \text{Tr}[\hat{\Gamma} \hat{n}_{\alpha}] = \frac{1}{Z} \sum_m \langle m | \hat{n}_{\alpha} | m \rangle e^{-\beta E_m}. \quad (5)$$

The density in turn uniquely determines the KS potential and thus the Hxc potential. In our case of an isolated QD at finite temperature the occupancy n_{α} is simply determined by the gate v_{α}^s of a non-interacting QD, and is thus simply given by the Fermi-Dirac distribution, i.e. $n_{\alpha} = 2 f(v_{\alpha}^s)$. Hence the KS gate for orbital α is given by $v_{\alpha}^s = \frac{1}{\beta} \ln\left(\frac{2}{n_{\alpha}} - 1\right)$ and the corresponding Hxc potential can be obtained using (4) as:

$$v_{\alpha}^{\text{Hxc}} = \frac{1}{\beta} \ln\left(\frac{2}{n_{\alpha}} - 1\right) - v_{\alpha}. \quad (6)$$

Hence we have found the mapping $\{n_{\alpha}\} \rightarrow \{v_{\alpha}^{\text{Hxc}}\}$. By exploring the parameter space $\{v_{\alpha}\}$ we can establish this mapping for the entire space of densities $\{n_{\alpha}\}$ (for $n_{\alpha} \in [0, 2]$).

A. Hxc potentials and link to stability diagrams for the double quantum dot

We now focus on the two-orbital case, i.e. a double quantum dot (DQD) with generic density-density interactions (U_1, U_2, U_{12}). For the moment we neglect Hund's rule coupling ($J_H = 0$), but we will discuss the effect of finite J_H later in Sec. IV C. The Hxc potentials can be constructed by reverse engineering as explained above. Here we are interested in the qualitative structure of the Hxc potentials, in particular in the positions (and heights) of step structures which appear in the low-temperature limit. In fact, these steps are not only the crucial but also the *only* features of the Hxc potential in the limit of low temperatures. In this section we will show how these step structures can be deduced completely from the stability diagrams.

A stability diagram highlights the occupations (densities) of the ground states in the different regions of the plane of external on-site energies v_1 and v_2 . The position and shape of these regions in the v_1 - v_2 plane depend on the values of the interaction parameters but within each region the pair of densities (n_1, n_2) remains constant at (close to) zero temperature and the possible values of the local densities n_i are restricted to 0, 1, and 2. These pairs of densities therefore give nine vertices in the n_1 - n_2 plane where, of course, for general temperatures the domain of physically realizable densities is restricted to the square $0 \leq n_i \leq 2$.

It turns out that the structure of the Hxc potentials (in the limit of low temperatures) for a given set of interaction parameters can be extracted just by looking at the stability diagram: for a given pair of ground state densities (or vertex) one just needs to find all adjacent regions corresponding to a different vertex. Then the Hxc potentials will *only* contain steps which connect a given vertex with those vertices corresponding to directly adjacent regions. The heights of these steps can also be extracted from the stability diagram. Below we will illustrate how this works presenting some representative examples and we will also explain the physical reasons behind our observations.

As a first example we choose a simple one where all interaction parameters are equal, $U_1 = U_2 = U_{12}$. In this case the total interaction can be written as $\frac{1}{2}U\hat{N}(\hat{N} - 1)$ where $\hat{N} = \hat{n}_1 + \hat{n}_2$ is the operator for the total number of electrons on the dot. This model is known as the constant interaction model (CIM). It can be shown⁴⁶ that at zero temperature the Hxc potential v_α^{Hxc} of the CIM is independent of α and is a piecewise constant function of the total electron number N with discontinuous steps of height U whenever N crosses an integer. We mention that the CIM Hxc potential is strictly discontinuous only at zero temperature (this is a manifestation of the famous derivative discontinuity of DFT¹⁰). At finite but small temperature, the step structure persists but the Hxc potentials are now continuous functions of the densities⁴⁷.

We now show how the known CIM Hxc potentials (at

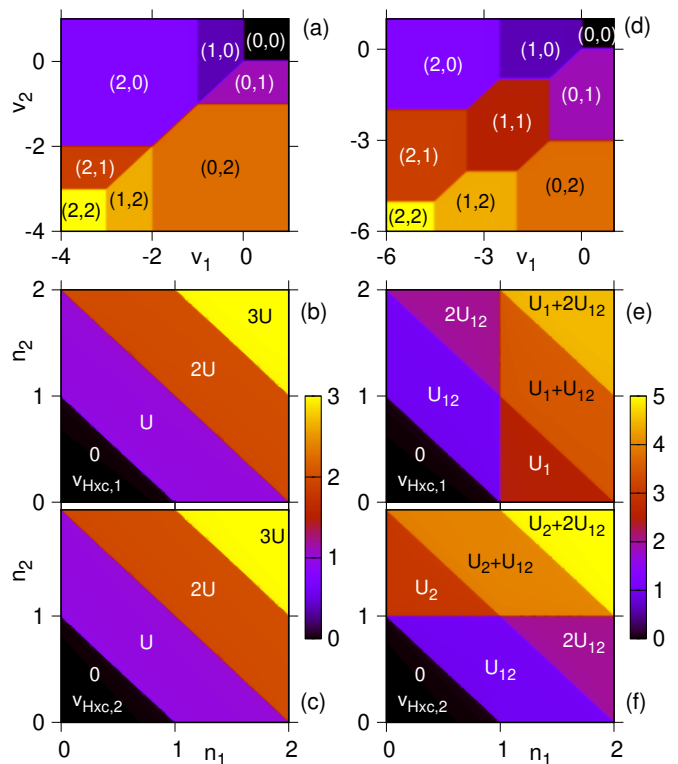


FIG. 1. Panels (a)-(c) (constant interaction model, CIM): stability diagram (a) and Hxc potentials for sites 1 and 2 (panels (b) and (c), respectively) of the double quantum dot for $U_1 = U_2 = U_{12}$. Panels (d)-(f) (Regime I): stability diagram (d) and Hxc potentials for sites 1 and 2 (panels (e) and (f), respectively) of the double quantum dot for $U_1 = 2.5U_{12}$, $U_2 = 3U_{12}$. All energies in units of smallest interaction (U_{12}).

low temperature) can be inferred directly from the stability diagram. This diagram is shown in panel (a) of Fig. 1 for the CIM with $U_1 = U_2 = U_{12} = 1$. Here the regions corresponding to the different possible ground state densities (given in parenthesis) are marked by different colors. The reverse-engineered Hxc potentials for sites 1 and 2 are shown in panels (b) and (c) of Fig. 1, respectively. In the stability diagram, the domain corresponding to the occupation (0, 0) is directly adjacent only to the domains with occupations (1, 0) and (0, 1). If we connect the (0, 0) vertex with one of those vertices in the n_1 - n_2 plane we see that the resulting lines run along the border of the allowed density domain. The complete set of lines along the borders of the density domain follow from the sequence of vertices $(0, 0) \rightarrow (1, 0) \rightarrow (2, 0)$, $(0, 0) \rightarrow (0, 1) \rightarrow (0, 2)$, $(2, 0) \rightarrow (2, 1) \rightarrow (2, 2)$, and $(0, 2) \rightarrow (1, 2) \rightarrow (2, 2)$. The only other possibilities of connecting vertices corresponding to adjacent regions in the $v_1 - v_2$ plane are (i) $(1, 0) \rightarrow (0, 1)$, (ii) $(2, 0) \rightarrow (0, 2)$, and (iii) $(2, 1) \rightarrow (1, 2)$. These lines are exactly the position of the steps at integer $N = n_1 + n_2$ in the Hxc potentials, see panels (b) and (c) of Fig. 1. Moreover, the height of these steps can also be deduced from the stability diagram: consider a $v_2 > 0$ such that the second dot is always empty, independent of

v_1 . Then we have essentially a single-site model (SSM) in contact with a particle and heat bath because the second dot doesn't contribute. However, we know that the Hxc potential of a SSM in the low temperature limit is a step function with step of height U at half filling⁴². In a self-consistent DFT calculation this step in the Hxc potential leads to a pinning of the KS level to the Fermi energy over a range of gates of width U . Therefore, the width (in v_1) of the (1,0) region is just $U_1 = U$. Similarly, the width (in v_2) of the (0,1) region is $U_2 = U$. The line in the stability diagram where the (1,0) and (0,1) regions touch is the line $v_1 = v_2$ for which the states with the corresponding occupations are degenerate. The KS system is a system of effectively non-interacting electrons which reproduces the interacting density. However, for a non-interacting double dot with on-site potentials v_1^s and v_2^s the *only* possibility for the half-filled dots to be degenerate is for the point $v_1^s = v_2^s = \ln 3/\beta$ which in the limit of zero temperature approaches $v_1^s = v_2^s = 0$. Therefore, in order to reproduce the degeneracy as observed in the stability diagram, the KS potential for *both* sites has to be pinned over an interval of range U . This can only be achieved if the Hxc potentials for both sites have steps at $N = 1$ of height U as observed in the reverse-engineered Hxc potentials. On the line $v_1 = v_2$ also the states with occupations (2,0) and (0,2) as well as the ones with occupations (2,1) and (1,2) are degenerate. It is easy to show that along this line the states with occupations (2,0) and (0,2) are lowest in energy for the region $-U > v_1 > -2U$. For non-interacting systems, again there is only one point ($v_1^s = v_2^s = 0$) for which the states with (2,0) and (0,2) are degenerate. Therefore, the Hxc potentials have to be such that for the range of gates $-U > v_1 > -2U$, the KS potentials are pinned to zero. This can only be achieved if both Hxc potentials exhibit a step of height U at $N = 2$, as observed. Finally, there is yet another step of height U in both Hxc potentials for $N = 3$ which follows in a similar way from the analysis of the contact line between the (2,1) and (1,2) regions. In this way we have therefore been able to reconstruct the Hxc potentials of the CIM only by analyzing the stability diagram.

In the second example we make all the interaction parameters different from each other, i.e., the levels are now not equivalent any more. Moreover, we choose the interdot interaction U_{12} to be smaller than both U_1 and U_2 . This parameter regime ($U_{12} < U_1, U_2$) we denote as Regime I, see discussion in Section IV A. In the stability diagram for this regime (panel (d) of Fig. 1) we now have a new region with densities (1,1) showing up. In order to deduce the low-temperature Hxc potentials (reverse-engineered results shown in panels (e) and (f) of Fig. 1), we begin by looking at the regions with occupations (1,0) and (0,1). The corresponding states are degenerate along the line $v_1 = v_2$ and for $-U_{12} < v_1 < 0$ they are the ground states of the double dot. For the KS system to reproduce this density for external potentials $v_1 = v_2$ in the same interval, we need the KS potentials on both

sites to be pinned to the Fermi energy. Therefore both Hxc potentials need to exhibit a step of height U_{12} along the line connecting the vertices (1,0) and (0,1). If one of the levels is completely empty, the other level essentially behaves like a SSM (see discussion of the previous example). Therefore, for the Hxc potential of site 1 we have $v_1^{\text{Hxc}}(n_1, 0) = U_1$ for $1 < n_1 < 2$ while $v_2^{\text{Hxc}}(0, n_2) = U_2$ for $1 < n_2 < 2$. The regions (1,0) and (1,1) are adjacent along the line $v_1 = -U_{12}$ for $-U_1 < v_1 < -U_{12}$ and thus the KS potential of the first site needs to be pinned to the Fermi energy for this range of v_1 leading to a step of height $U_1 - U_{12}$ along the line connecting the (1,0) and (1,1) vertices for v_1^{Hxc} . Similarly, v_2^{Hxc} needs to exhibit a step of height $U_2 - U_{12}$ along the line connecting the (0,1) and (1,1) vertices. Next, the regions (2,0) and (1,1) are adjacent for $-U_{12} - U_\alpha < v_\alpha < -U_\alpha$ ($\alpha = 1, 2$) and therefore both Hxc potentials have a step of height U_{12} along the lines connecting the (2,0) and (1,1) vertices. Similarly, there also has to be a step of height U_{12} in both Hxc potentials along the line connecting the (0,2) and (1,1) vertices. The regions (1,1) and (1,2) are adjacent for $-2U_{12} < v_1 < -U_1 - U_{12}$ leading to a step of height $U_1 - U_{12}$ in v_1^{Hxc} along the line (1,1) \rightarrow (1,2). Similarly, there is a step of height $U_1 - U_{12}$ in v_2^{Hxc} along the (1,1) \rightarrow (2,1) line. Finally, the regions (2,1) and (1,2) are adjacent along a line of length U_{12} leading to a step of this height in both Hxc potentials along the (2,1) \rightarrow (1,2) line. In this way we now have completely determined the (low temperature) Hxc potentials of both sites just by analyzing the stability diagram. Their overall structure is such that they exhibit steps for integer total occupation $N = n_1 + n_2$ for both Hxc potentials plus an additional step at $n_\alpha = 1$ for v_α^{Hxc} . Note also that for the special case $U_{12} = 0$ only the steps at $n_\alpha = 1$ for v_α^{Hxc} survive while those at integer N disappear. This is not surprising since in this case our model just describes two completely independent single impurities and, naturally, the corresponding Hxc potential for site α is completely independent of the other site and given by the Hxc potential of a SSM with interaction strength U_α . This has also been discussed as ‘‘intra-system steps’’ in Ref. 48.

We have identified two further parameter regimes for the interaction parameters (see Section IV A) where qualitative changes both in the stability diagram as well as in the Hxc potentials occur. In both regimes the inter-orbital interaction U_{12} is smaller than at least one of the intra-orbital ones. Without loss of generality we may assume $U_1 \leq U_2$. In Regime II we have $U_1 < U_{12} < (U_1 + U_2)/2$ while Regime III is defined by $U_1 \leq (U_1 + U_2)/2 \leq U_{12}$. In panels (a)-(c) of Fig. 2 we show the stability diagram and Hxc potentials for interaction parameters chosen in Regime II. Compared to Regime I (panels (d)-(f) of Fig. 1), in the stability diagram we now find that there exists a range of on-site potentials for which regions (2,0) and (0,1) are directly adjacent and, similarly, for the regions (2,1) and (0,2). As expected, these transitions lead to the new steps in the Hxc potentials. On the other hand, for the Hxc po-

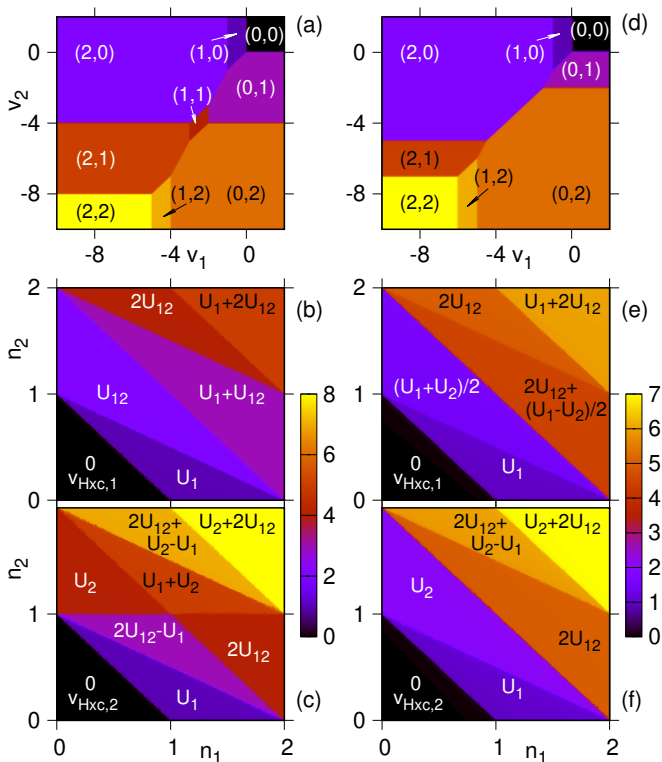


FIG. 2. Panels (a)-(c) (Regime II): stability diagram (a) and Hxc potentials for sites 1 and 2 (panels (b) and (c), respectively) of the double quantum dot for $U_2 = 4U_1$ and $U_{12} = 2U_1$. Panels (d)-(f) (Regime III): stability diagram (d) and Hxc potentials for sites 1 and 2 (panels (e) and (f), respectively) of the double quantum dot for $U_2 = 2U_1$, and $U_{12} = 2.5U_1$. All energies in units of the smallest interaction (U_1).

tential of site 1 the step at $n_1 = 1$ (present in Regime I) now disappears while in $v_{\text{Hxc},2}$ the step at $n_2 = 1$ survives (this step is related to the vertical lines delimiting the (1,1) region in the stability diagram). We have annotated the plateau values in both Hxc potentials which can be found by analyzing the stability diagram using similar arguments to the ones used above for Regime I.

Finally, in panels (d)-(f) of Fig. 2 we show the stability diagram and Hxc potentials for interaction parameters chosen in Regime III. Compared to Regime II, the main qualitative difference is the disappearance of the step at $n_2 = 1$ in the Hxc potential of site 2. Again, all the step structures in the Hxc potentials can fully be deduced by analyzing the stability diagram.

Before we close this section we would like to mention that for multilevel dots beyond the double dot studied here, in principle the analysis of the (multidimensional) stability diagram(s) also allows for a complete deduction of the low-temperature Hxc potentials of the different sites. However, it is clear that this procedure rapidly becomes quite cumbersome as the number of levels increases.

IV. MODELLING OF THE HXC POTENTIALS

A. Decomposition of the interaction into basic building blocks

In the following we show that the Hxc potentials for generic density-density interactions can be built from a few basic potentials. We start with the most common (or natural) situation where the inter-orbital interaction U_{12} is smaller than both of the intra-orbital ones, $U_{12} \leq U_1, U_2$. A specific case with $U_{12} < U_1 < U_2$ was studied in the previous section [see Fig. 1(d-f)]. The corresponding Hxc potential shows steps at integer values of $N = n_1 + n_2$, connected to a CIM potential, as well as steps at $n_1 = 1$ for orbital 1 or at $n_2 = 1$ for orbital 2 connected to a SSM potential of the corresponding orbital.

This suggests that in the regime $U_{12} \leq U_1, U_2$ the Hxc potential for each orbital may be built from a superposition of a CIM potential plus a SSM potential. We can rationalize this idea by a decomposition of the Coulomb interaction term as follows. Rewriting the inter-orbital repulsion as

$$U_{12} \hat{n}_1 \hat{n}_2 = \frac{U_{12}}{2} \hat{N}(\hat{N} - 1) - U_{12} \sum_{\alpha} \hat{n}_{\alpha\uparrow} \hat{n}_{\alpha\downarrow} \quad (7)$$

we can split the interaction into a CIM part and two SSM interactions (one for each orbital):

$$\mathcal{V}_{\text{int}} = \frac{1}{2} U_{12} \hat{N}(\hat{N} - 1) + \sum_{\alpha} \delta U_{\alpha} \hat{n}_{\alpha\uparrow} \hat{n}_{\alpha\downarrow} \quad (8)$$

where $\delta U_{\alpha} \equiv U_{\alpha} - U_{12}$ is the “excess interaction” for each orbital. This suggests to write the Hxc potential for level α for **Regime I** ($U_{12} \leq U_1, U_2$) as the sum of the CIM Hxc potential for interaction U_{12} and the SSM potential for δU_{α} :

$$v_{\alpha}^{\text{Hxc}}[n_1, n_2] = v_{\text{CIM}}^{\text{Hxc}}(U_{12})[n_1 + n_2] + v_{\text{SSM}}^{\text{Hxc}}(\delta U_{\alpha})[n_{\alpha}]. \quad (9)$$

Now if U_{12} is larger than at least one of the intra-orbital interactions U_{α} this decomposition of the Coulomb interaction obviously leads to negative interactions δU_{α} in the SSM parts. Since the step in the Hxc potential of the SSM at $n_{\alpha} = 1$ would actually vanish for negative interactions,⁴⁹ in this regime the step structure can obviously not be rationalized by the above decomposition of the interaction. Indeed the structure of the reverse-engineered Hxc potentials (Fig. 2) appears to be quite different from that for the regime $U_{12} \leq U_{\alpha}$. Essentially, two new features are found in this regime: (i) an increase of the step height at $N = 2$ with respect to the CIM potential, and (ii) peculiar new steps at integer values of $n_1/2 + n_2$. The steps at integer $n_1/2 + n_2$ are generated by a peculiar interaction of the form

$$\mathcal{V}_{\text{skew}} = \frac{U}{2} \hat{n}_2(\hat{N} - 1) \quad (10)$$

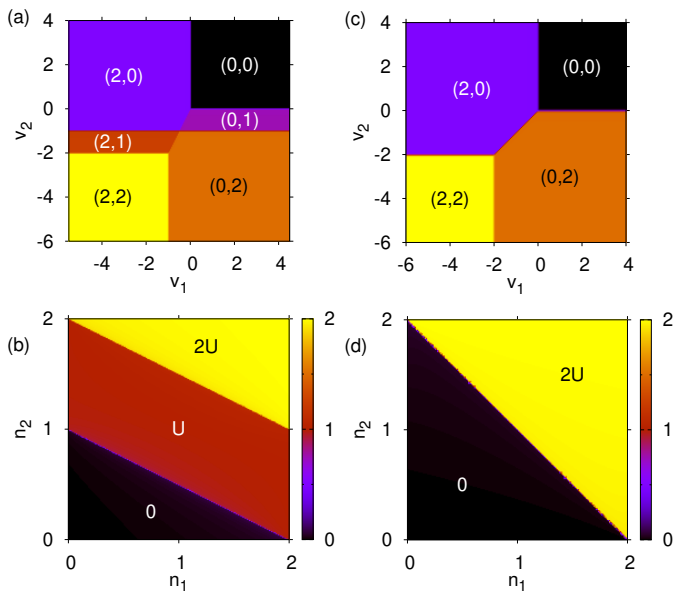


FIG. 3. (a,b) Stability diagram (a) and Hxc potential of orbital 2 (b) for the Skew interaction $\mathcal{V}_{\text{skew}} = \frac{U}{2}\hat{n}_2(\hat{N} - 1)$. The structure of the Hxc potential for orbital 1 is the same as for orbital 2 but the step heights are half those of orbital 2 (0, $U/2$, U). (c,d) Stability diagram (c) and Hxc potential of both orbitals (d) for the inter-orbital interaction $\mathcal{V}_{\text{inter}} = U\hat{n}_1\hat{n}_2$. All energies in units of U in both cases.

which we will refer to as *Skew interaction* from now on. This interaction is realized by setting $U_1 = 0$ and $U_{12} = U_2/2 = U/2$. The corresponding stability diagram and the Hxc potential for orbital 2 is shown in Fig. 3(b). Note that the Hxc potential of orbital 1 has the same structure but the step heights are lower by a factor of $1/2$.

Common to all cases is that there is always a contribution of the CIM potential, as long as all interactions (U_1, U_2, U_{12}) remain finite. This contribution is given by the smallest interaction. In the case that U_{12} is larger than at least one of the intra-orbital interactions U_α , we may assume without loss of generality that U_1 is the smallest interaction. Subtracting the CIM interaction $\sim U_1$ from the total interaction thus yields:

$$\begin{aligned} \mathcal{V}_{\text{int}} - \frac{U_1}{2}\hat{N}(\hat{N} - 1) &= \\ &= (U_{12} - U_1)n_1n_2 + (U_2 - U_1)n_{2\uparrow}n_{2\downarrow} \\ &= (U_{12} - U_1)n_1n_2 + \frac{U_2 - U_1}{2}n_2(n_2 - 1) \quad (11) \end{aligned}$$

where in the last term we have rewritten the intra-orbital interaction for orbital 2 in terms of $n_2 = n_{2\uparrow} + n_{2\downarrow}$ instead of $n_{2\uparrow}$ and $n_{2\downarrow}$. Hence the remaining interaction consists of an inter-orbital interaction $\sim (U_{12} - U_1)$ and a SSM interaction $\sim (U_2 - U_1)/2$ for orbital 2. These two terms can be combined to yield the Skew interaction and a remaining term. Depending on whether $U_{12} - U_1$ is larger or smaller than $(U_2 - U_1)/2$, the remaining term is either a SSM interaction for orbital 2 if $U_{12} - U_1 < (U_2 - U_1)/2$

(or equivalently $U_{12} < U_{\text{ave}} \equiv (U_1 + U_2)/2$) or an inter-orbital interaction if $U_{12} - U_1 > (U_2 - U_1)/2$ (or equivalently $U_{12} > U_{\text{ave}}$).

We thus identify two new regimes in addition to Regime I ($U_{12} \leq U_\alpha$) discussed above: In **Regime II** the inter-orbital interaction U_{12} takes values between the lowest interaction of both intra-orbital interactions and their average U_{ave} , i.e. $U_1 < U_{12} < U_{\text{ave}}$. This is the case shown in Fig. 2(a-c). After subtraction of the CIM potential $\sim U_1$ we find that the remaining interaction in Regime II can be written as

$$(U_{12} - U_1)\hat{n}_2(\hat{N} - 1) + 2(U_{\text{ave}} - U_{12})\hat{n}_{2\uparrow}\hat{n}_{2\downarrow}. \quad (12)$$

Overall this suggests the following decomposition of the Hxc potential in **Regime II** ($U_1 < U_{12} < U_{\text{ave}}$):

$$\begin{aligned} v_\alpha^{\text{Hxc}}[n_1, n_2] &= v_{\text{CIM}}^{\text{Hxc}}(U_1)[n_1 + n_2] \\ &+ v_{\text{skew},\alpha}^{\text{Hxc}}(2(U_{12} - U_1))[n_1, n_2] \\ &+ v_{\text{SSM}}^{\text{Hxc}}(2(U_{\text{ave}} - U_{12}))[n_2]\delta_{\alpha 2} \quad (13) \end{aligned}$$

where $\delta_{\alpha 2}$ is the Kronecker-delta which ensures that the SSM term only contributes to the Hxc potential of orbital 2. Note that as $U_{12} \rightarrow U_{\text{ave}}$ the SSM term vanishes.

On the other hand **Regime III** occurs when the inter-orbital interaction exceeds the average intra-orbital interaction, i.e. $U_{12} > U_{\text{ave}} > U_1$. This was the case considered in Fig. 2(d-f). In this regime the remaining interaction after subtraction of the CIM $\sim U_1$ can be rewritten in terms of the Skew interaction (10) and a pure inter-orbital interaction part:

$$\frac{U_2 - U_1}{2}\hat{n}_2(\hat{N} - 1) + (U_{12} - U_{\text{ave}})\hat{n}_1\hat{n}_2. \quad (14)$$

As can be seen in Fig. 3(d), this inter-orbital term

$$\mathcal{V}_{\text{inter}} = U\hat{n}_1\hat{n}_2 \quad (15)$$

gives rise to a single step at $N = 2$ which explains the increase in step height at $N = 2$ with respect to the CIM, observed in Fig. 2(e,f). Overall this suggests the following decomposition of the Hxc potential in **Regime III** ($U_{12} > U_{\text{ave}} > U_1$):

$$\begin{aligned} v_\alpha^{\text{Hxc}}[n_1, n_2] &= v_{\text{CIM}}^{\text{Hxc}}(U_1)[n_1 + n_2] \\ &+ v_{\text{skew},\alpha}^{\text{Hxc}}(U_2 - U_1)[n_1, n_2] \\ &+ v_{\text{inter}}^{\text{Hxc}}(U_{12} - U_{\text{ave}})[n_1 + n_2]. \quad (16) \end{aligned}$$

We can see that for $U_1 = U_2$ the Skew part of the Hxc potential disappears.

Hence we have found a decomposition of the Hxc potential for a two-orbital model with generic (density-density) interactions in all three regimes in terms of four basic potentials which are shown schematically in Fig. 4. We would like to emphasize at this point that **Regime I** corresponds to a more natural choice of parameters than the other two regimes, since the inter-orbital interaction U_{12} is generally smaller than any of the intra-orbital interactions U_α . Nevertheless, the other regimes might be

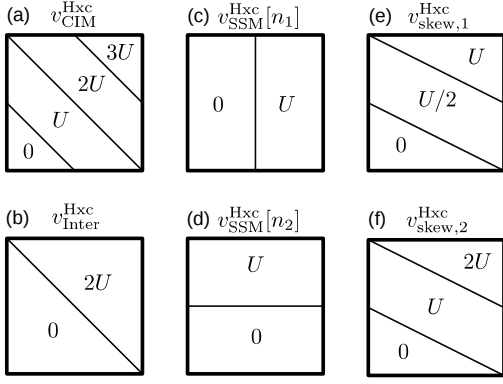


FIG. 4. Schematic representation of the four basic Hxc potentials for building the generic potentials for all three regimes. (a) Hxc potential for CIM interaction $\frac{U}{2}\hat{N}(\hat{N} - 1)$. (b) Hxc potential for inter-orbital interaction Un_1n_2 . (c,d) Hxc potential for intra-orbital (i.e. SSM) interactions $Un_{\alpha\uparrow}n_{\alpha\downarrow}$. (e,f) Hxc for the Skew interaction $\frac{U}{2}\hat{n}_2(\hat{N} - 1)$.

realized by effective models or possibly by screening of the Coulomb interactions. In the next section we will present parametrizations of the Hxc potentials in the different regimes, making use of its decomposition into the basic building blocks shown in Fig. 4.

B. Generalization of Hxc potential to more than two orbitals

For specific choices of parameters we can generalize the Hxc potential for the DQD to an arbitrary number of orbitals in a straightforward manner. We concentrate on the physically most relevant **Regime I** ($U_\alpha, U_\beta > U_{\alpha\beta}$). If we choose the inter-orbital interaction to be constant, $U_{\alpha\beta} \equiv U'$, which thus has to be smaller than *all* of the intra-orbital interactions, $U' < U_\alpha$, we can rewrite the interaction in a similar manner as in Eq. (8) in terms of a CIM term $\sim U'$ for all the electrons $N = \sum_\alpha n_\alpha$ and SSM terms $\sim \delta U_\alpha \equiv U_\alpha - U'$ for the individual orbitals as

$$\mathcal{V}_{\text{int}} = \frac{1}{2}U'\hat{N}(\hat{N} - 1) + \sum_\alpha \delta U_\alpha \hat{n}_{\alpha\uparrow}\hat{n}_{\alpha\downarrow} \quad (17)$$

where $\delta U_\alpha = U_\alpha - U'$. This suggests to decompose the XC functionals in complete analogy to the two-orbital case in Regime I as

$$v_\alpha^{\text{Hxc}}\{n_\alpha\} = v_{\text{CIM}}^{\text{Hxc}}(U')[N] + v_{\text{SSM}}^{\text{Hxc}}(\delta U_\alpha)[n_\alpha]. \quad (18)$$

In Sec. VB we will see that this decomposition of the Hxc potential leads to excellent results for multi-orbital QDs. For a more general choice of interaction parameters, the above decomposition is likely to become more complicated. This will be the focus of future work.

C. The effect of Hund's rule coupling

So far we have neglected the effect of Hund's rule coupling on the Hxc potentials. In Fig. 5 we show the stability diagram and the corresponding reverse-engineered Hxc potential for the case of a CIM type direct interaction part ($U_1 = U_2 = U_{12}$) plus the full Hund's coupling contribution (J_H). Both the stability diagram and the reverse-engineered Hxc potential shown in Fig. 5 resemble the ones for the case with $U_{12} < U_\alpha$ without Hund's coupling (cf. Fig. 1(d-f)). Only the size of the vertex regions changes in the stability diagram, and correspondingly in the Hxc potentials only the step heights change. Moreover, by switching off the spin-flip term in (1) we find that it does not have any effect on the densities and consequently on the Hxc potentials and thus can be neglected. Hence in the following considerations we only need to take into account the density-density part of the Hund's coupling in (next to last term in Eq. 1).

In the spirit of the previous section we can rewrite the density-density part of the Hund's rule coupling term in terms of a (negative) CIM interaction and (positive) SSM interactions for the remaining orbitals plus a remaining *positive* interaction part:

$$\begin{aligned} \mathcal{V}_H &= -J_H \sum_\sigma \hat{n}_{1\sigma}\hat{n}_{2\sigma} = -J_H\hat{n}_1\hat{n}_2 + J_H \sum_\sigma \hat{n}_{1\sigma}\hat{n}_{2\bar{\sigma}} \\ &= -\frac{J_H}{2}\hat{N}(\hat{N} - 1) + J_H \sum_\alpha \hat{n}_{\alpha\uparrow}\hat{n}_{\alpha\downarrow} + J_H \sum_\sigma \hat{n}_{1\sigma}\hat{n}_{2\bar{\sigma}} \end{aligned} \quad (19)$$

where in the last term $\bar{\sigma}$ denotes the opposite spin of σ . The last term gives rise to a step at $N = 2$ of height J_H in the Hxc potential similar to the inter-orbital interaction term but with step height J_H instead of $2U$ (cf. Fig. 3(d)).

When adding the density-density contribution of the Hund's rule coupling to the direct interaction part in Regime I ($U_{12} \leq U_1, U_2$), we can rewrite the interaction in terms of a CIM interaction, SSM terms, and the last term of the Hund density-density interaction (19) as

$$\begin{aligned} \mathcal{V}_{\text{int}} &= \frac{U_{12} - J_H}{2}\hat{N}(\hat{N} - 1) + \sum_\alpha (\delta U_\alpha + J_H)\hat{n}_{\alpha\uparrow}\hat{n}_{\alpha\downarrow} \\ &\quad + J_H \sum_\sigma \hat{n}_{1\sigma}\hat{n}_{2\bar{\sigma}} \end{aligned} \quad (20)$$

where as defined in the previous section $\delta U_\alpha = U_\alpha - U_{12}$. Hence all terms can be modeled by the basic Hxc potentials shown in Fig. 4:

$$\begin{aligned} v_\alpha^{\text{Hxc}}[n_1, n_2] &= v_{\text{CIM}}^{\text{Hxc}}(U_{12} - J_H)[n_1 + n_2] \\ &\quad + v_{\text{SSM}}^{\text{Hxc}}(\delta U_\alpha + J_H)[n_1, n_2] \\ &\quad + v_{\text{inter}}^{\text{Hxc}}(J_H/2)[n_1 + n_2]. \end{aligned} \quad (21)$$

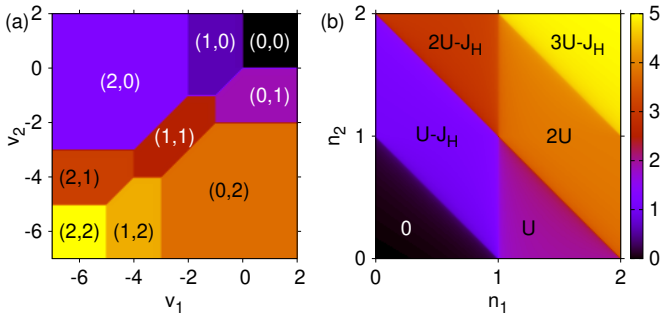


FIG. 5. Effect of Hund's rule coupling on (a) Stability diagram and (b) Hxc potential of orbital 1 for CIM interaction plus Hund's rule coupling, $\mathcal{V}_{\text{int}} = \frac{U}{2}\hat{N}(\hat{N} - 1) + \mathcal{V}_{\text{Hund}}$ for $U = 2J_H$. Here due to symmetry the Hxc potential for orbital 2 can simply be obtained by reflection along the $n_1 = n_2$ line. All energies in units of J_H .

D. Parametrization of the basic Hxc potentials

In the zero temperature limit, the steps in the Hxc potential become infinitely sharp and thus can be described by simple step functions. At finite temperature, however, the steps are broadened in a non-trivial way. For the SSM at finite temperature an *exact* expression for the Hxc potential can be derived:⁴⁷

$$v_{\text{SSM}}^{\text{Hxc}}[n] = U + \frac{1}{\beta} \ln \left(\frac{x + \sqrt{x^2 + e^{-\beta U}(1 - x^2)}}{1 + x} \right) \quad (22)$$

where $x = n - 1$.

In the following we will use the Hxc functional for the SSM as the basis for constructing approximations for the other three basic Hxc potentials into which the generic Hxc potential can be decomposed, namely the CIM, the Inter-orbital, and the Skew potential (see Fig. 4). We start with the CIM potential and show that an excellent parametrization of the Hxc potential can be achieved by simply summing the (exact) SSM potential (22) over the charging states of the dot, and shifting and rescaling it such that the potential does not become negative or larger than $(2\mathcal{M} - 1)U$:

$$v_{\text{CIM}}^{\text{Hxc}}[N] = \frac{(2\mathcal{M} - 1)U}{v_{\text{CIM}}^{\text{max}}} \times \sum_{J=1}^{2\mathcal{M}-1} [v_{\text{SSM}}^{\text{Hxc}}[N - J + 1] - v_{\text{SSM}}^{\text{Hxc}}[-J + 1]] \quad (23)$$

where

$$v_{\text{CIM}}^{\text{max}} = \sum_{J=1}^{2\mathcal{M}-1} [v_{\text{SSM}}^{\text{Hxc}}[2\mathcal{M} - J + 1] - v_{\text{SSM}}^{\text{Hxc}}[-J + 1]] \quad (24)$$

is the maximal value that the sum in (23) acquires at $N = 2\mathcal{M}$. The prefactor $(2\mathcal{M} - 1)U/v_{\text{CIM}}^{\text{max}}$ thus rescales the potential such that the potential yields the exact value

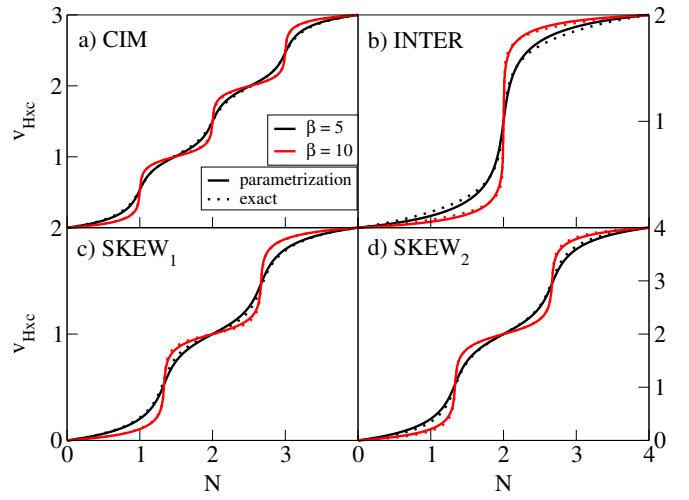


FIG. 6. Comparison of parametrized and exact Hxc potentials as a function of $N = n_1 + n_2$ for three basic interactions: (a) CIM interaction ($U_1 = U_2 = U_{12} > 0$); (b) Inter-orbital interaction ($U_{12} > 0$ and $U_1 = U_2 = 0$); (c) Skew interaction ($U_2 = 2U_{12} > 0$ and $U_1 = 0$); All energies in units of the smallest non-zero interaction (U_{12}).

$(2\mathcal{M} - 1)U$ at $N = 2\mathcal{M}$. As can be seen in Fig. 6(a), the agreement with the exact result is quite remarkable.

For the inter-orbital potential we find a good parametrization describing the step at total $N = 2$ again in terms of the SSM potential, as

$$v_{\text{inter}}^{\text{Hxc}}(U, \beta)[N] = v_{\text{SSM}}^{\text{Hxc}}(2U, \beta^*)[N/2] \quad (25)$$

where we have replaced the actual inverse temperature β by an effective reduced value, $\beta^* = 0.73\beta$ and the step height is increased by a factor of 2 compared to the SSM. The agreement with the exact potential is very good as can be seen in Fig. 6(b).

Finally, for the Skew interaction, we parametrize the Hxc potential in a similar way as the Hxc potential for the CIM, by summing two SSM potentials, one for each of the steps, and shifting and rescaling so that the potential does not become negative or larger than the maximum value:

$$v_{\text{skew},\alpha}^{\text{Hxc}}(U)[n_1, n_2] = \frac{\alpha U}{v_{\text{skew}}^{\text{max}}} \sum_{J=0,1} \{v_{\text{SSM}}^{\text{Hxc}}(\frac{U}{2})[\frac{n_1}{2} + n_2 - J] - v_{\text{SSM}}^{\text{Hxc}}(\frac{U}{2})[-J]\} \quad (26)$$

where

$$v_{\text{skew}}^{\text{max}} = \sum_{J=0,1} \{v_{\text{SSM}}^{\text{Hxc}}(\frac{U}{2})[3 - J] - v_{\text{SSM}}^{\text{Hxc}}(\frac{U}{2})[-J]\}. \quad (27)$$

Also here the agreement with the exact potential is very good as can be seen in Figs. 6(c+d).

We have thus found parametrizations of the four basic Hxc potentials. It should be noted, however, that at higher temperatures the exact CIM and Inter-orbital potentials (which in the zero temperature limit only depend

on total N) acquire also a dependence on the difference $\delta N \equiv n_1 - n_2$ which has not been taken into account here. This discrepancy of our parametrizations might be responsible for some of the moderate deviations of our DFT results from the exact ones discussed in the next section.

V. DFT CALCULATIONS

We are now going to apply the above developed parametrization of the Hxc potential in actual DFT calculations. To this end we solve the KS equations which for the multi-orbital QD in the GCE are given by:

$$n_\alpha = 2 f(v_\alpha + v_{\text{Hxc}}[\{n_{\alpha'}\}]) \text{ for } \alpha = 1 \dots \mathcal{M}. \quad (28)$$

Since the sharp step features in the Hxc potentials are expected to prevent the convergence of the usual self-consistency procedure in the density,⁵⁰ here we make use instead of a multidimensional generalization of the bisection approach as proposed before in Ref. 50 for finding the root of the multidimensional function

$$F_\alpha[\{n_{\alpha'}\}] \equiv n_\alpha - 2 f(v_\alpha + v_{\text{Hxc}}[\{n_{\alpha'}\}]). \quad (29)$$

In the following we study the evolution of the density $\{n_\alpha\}$ of multi-orbital QDs as a function of the applied gate v_g for different parameter sets. The gate v_g exerts a total shift of the QD levels ϵ_α and hence the total gate for orbital α is given by

$$v_\alpha = \epsilon_\alpha + v_g. \quad (30)$$

Consequently, the differences in the gate potentials between different orbitals remain constant as the gate v_g changes, $\delta v_{\alpha\beta} \equiv v_\alpha - v_\beta = \epsilon_\alpha - \epsilon_\beta$. In the following we will usually take the particle-hole symmetric (phs) point given by $\epsilon_\alpha^* = -\frac{U_\alpha}{2} - \sum_{\beta \neq \alpha} U_{\alpha\beta}$ as the reference system.

A. Results for the double quantum dot

We now study the DQD, and start by considering the degenerate case in Regime I, i.e. $U_1 = U_2 > U_{12}$ where $\delta N = 0$. Fig. 7 compares the exact densities with the ones computed in DFT using the Hxc potential for Regime I, Eq. (9), together with the parametrizations of the SSM, Eq. (22), and the CIM, Eq. (23), respectively. We see that the DFT results correctly describe all the features of the densities as a function of gate. At low temperatures, the width of the central step (around $v_g = 0$) is given by U_i while the other two step widths correspond to U_{12} . At higher temperatures our parametrization leads to moderate discrepancies in the slopes of the central step that disappear as the temperature approaches zero.

Next we consider the situation where the intra-orbital Coulomb repulsions are different, $U_1 > U_2 > U_{12}$. In Fig. 8(a,b), the occupations n_i are presented as a function of the gate v_g for two different temperatures. At

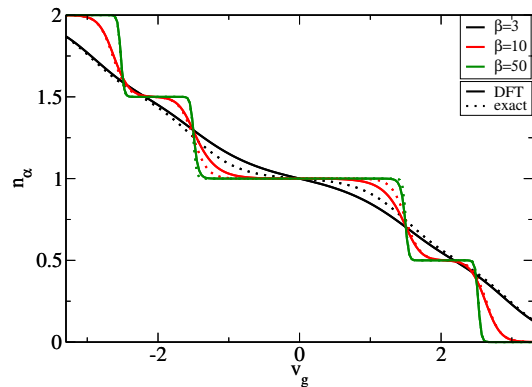


FIG. 7. Density $\{n_1, n_2\}$ as function of the gate voltage v_g for different temperatures when $U_1 = U_2 = 3U_{12} > 0$ (Regime I). The DFT result (solid line) becomes on top of the GCE result (dashed line) in the low temperature regime. All energies in units of the smallest interaction U_{12} .

low temperatures [Fig. 8(a)] at large negative gate voltage ($v_g < -2.5$) both orbitals of the DQD are completely filled ($n_\alpha \sim 2$). As the gate is increased, first the orbital with the higher interaction (U_1) becomes half-filled around $v_g \sim -2.5$, and then around $v_g \sim -1.5$ also the orbital with the lower interaction (U_2) becomes half-filled. Upon further increase of the gate, the sequence of emptying is reversed, as first the orbital with the higher interaction and thus lower gate (v_2) is emptied around $v_g \sim 1.5$ and finally the orbital with lower interaction and thus higher gate (v_1) is emptied. At higher temperatures extra steps develop in the evolution of the density versus gate voltage, as can be seen in Fig. 8(b). The appearance of new steps can be understood by the path taken in the $n_1 - n_2$ plane as the gate voltage changes, shown in the inset of Fig. 8(b) for different temperatures. At low temperatures the path essentially follows three straight line segments, along the lower border, across the plane and finally along the upper border, thus avoiding extra steps of the CIM potential at $N = 1$ and $N = 3$. As the temperature increases the path becomes smoother, and passes through the $N = 1$ and $N = 3$ steps of the CIM potential, leading to the extra steps in the evolution of the densities at higher temperature. While for low temperatures the agreement of the DFT results with the exact ones is excellent, at higher temperatures deviations appear. Although DFT qualitatively captures the appearance of the extra steps in the evolution of the density versus gate voltage, their heights are not correctly reproduced in DFT. Presumably this discrepancy can be attributed to the development of a δN -dependence of the CIM potential at finite temperature, and will be addressed in future work.

Finally, we turn our attention to Regimes II and III, which are both characterized by the appearance of the peculiar ‘‘Skew’’ term in the Hxc potential. Fig. 9(a) directly compares the evolution of the density as a function of the gate in both regimes. As we can see the behaviour

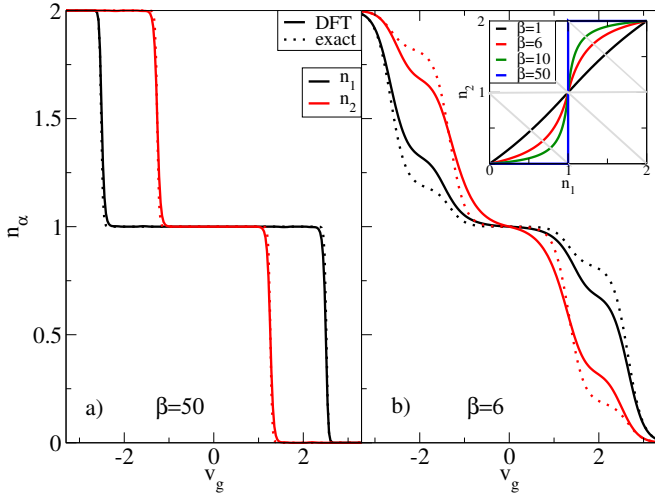


FIG. 8. Density $\{n_1, n_2\}$ as a function of the gate voltage v_g for $U_1 = 3U_{12}$, $U_2 = 2.5U_{12}$ (Regime I) for (a) low and (b) high temperatures. The inset of panel (b) shows the path in the $n_1 - n_2$ plane as the gate is varied for different temperatures. The grey lines show the steps of the CIM and SSM terms that appear in the Hxc potentials. All energies in units of the smallest interaction U_{12} .

is actually quite similar for both regimes, and not so different from Regime I (cf. Fig. 8): As the gate increases, first the orbital with the higher interaction (here U_2) becomes half-filled, and then the orbital with the lower interaction (U_1). Then upon further increase of the gate, the order of emptying is reversed. Due to the higher inter-orbital interaction in Regime III, the width of the central plateau is increased for both orbitals. Again, at low temperature the agreement with the exact results is excellent, but at higher temperatures moderate quantitative deviations occur (not shown).

In order to investigate the influence of the Skew term in the Hxc potential on the evolution of the densities, we next concentrate on Regime II and explore different paths in the $n_1 - n_2$ plane. To this end we fix the energy splitting $\delta v = v_1 - v_2$ between the orbitals to different values while the total gate changes, i.e. $v_1 = \delta v + v_g$ and $v_2 = v_g$. Fig. 9(b) shows the evolution of the density for two different values of δv and correspondingly different paths in the $n_1 - n_2$ plane (shown in the inset). For $\delta v = 0$ we observe an interesting effect. As the gate increases, the occupation of orbital 2 decrease in two steps, first to half filled and then further to zero, while the first orbital remains fully occupied. Then around $v_g = -1$ the occupation of orbital 1 decreases abruptly to quarter filling, while now the occupation of orbital 2 increases again to quarter filling, $n_1 = n_2 = \sim 0.5$. This non-monotonic behaviour of the occupation of orbital 2 is reminiscent of the so-called level occupation switching (LOS)^{51,52}. We find similar behaviour in Regime III (not shown).

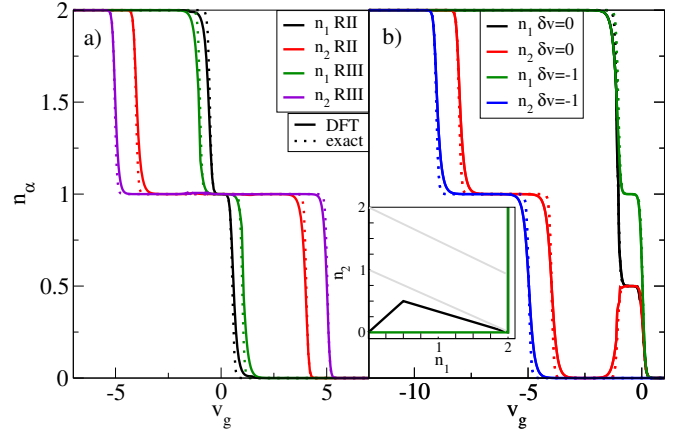


FIG. 9. (a) Comparison of the evolution of the density $\{n_1, n_2\}$ with the gate voltage v_g in Regime II ($U_2 = 2U_{12} = 4U_1$) and Regime III ($U_2 = U_{12} = 4U_1$). (b) Comparison of density evolution for different two different values of the splitting δv in Regime II ($U_{12} = 2U_1$). The inset shows the different paths in the density plane. $\beta = 20/U_1$ everywhere. All energies in units of U_1 .

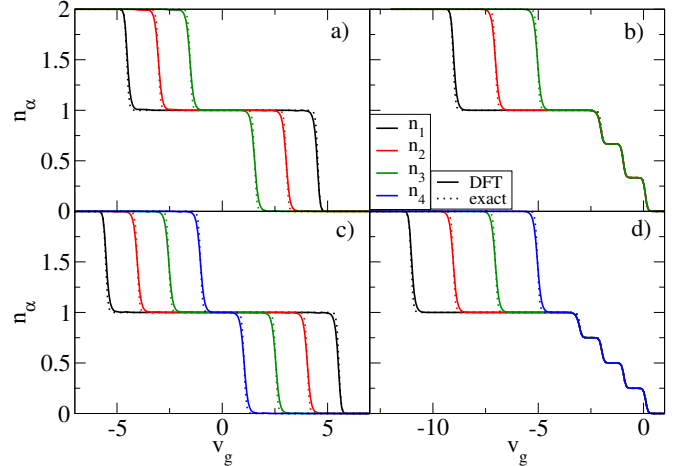


FIG. 10. Local occupations for the triple (a, b) and quadruple (c, d) QD as function of the gate voltage. In the left panels the QD levels are taken at particle-hole ($v_\alpha = \epsilon_\alpha^* + v_g$) and in the right the impurities level is set to zero ($v_\alpha = v_g$). $\beta = 20/U'$ and $U_1 = 5U'$, $U_2 = 4U'$, $U_3 = 3U'$, $U_4 = 2U'$. All energies in units of U' .

B. Results for more than two orbitals

Finally we apply the generalization of the Hxc potential (18) for more than two orbitals to DFT calculations of multi-orbital QDs. Fig. 10 shows the evolution of the density $\{n_\alpha\}$ as a function of the applied gate voltage v_g for three (a,b) and four-level (c,d) QD with all intra-orbital Coulomb repulsions U_α different and constant inter-dot repulsion $U'(U_1 > U_2 > \dots > U')$ at low temperature. In panels (a) and (c) the gate v_g is applied w.r.t. the phs point, i.e. $\epsilon_\alpha^* = -\frac{U_\alpha}{2} - \sum_{\beta \neq \alpha} U_{\alpha\beta}$. In this case

the path in the three- or four-dimensional density space avoids the steps in the CIM Hxc potential away from half-filling ($N = \mathcal{M}$) resulting in only three plateaus in the density evolution with the gate, in a similar way as in the DQD [cf. Fig. 8(a)]. On the other hand, in panels (b) and (d) (where $\epsilon_\alpha = 0$ and thus $\delta v_{\alpha\beta} = 0$) two (three) extra steps related to the inter-orbital Coulomb repulsions appear in the triple (quadruple) QD. The agreement between the DFT and the exact results is remarkable in all cases, showing that the generalization of Eq. (18) of the Hxc potential to more than two orbitals is valid. Finding similar expressions for a more general choice of parameters will be the focus of future work.

VI. CONCLUSIONS

In this work we have obtained Hxc potentials for double quantum dots in the grand-canonical ensemble subject to generic density-density interactions and Hund's rule coupling by reverse-engineering from exact many-body solutions. The structure of the Hxc potentials consists of ubiquitous steps whose exact positions depend on the regime defined by the interaction parameters. This structure can be understood and derived from an analysis of the stability diagrams. In a second step we were able to rationalize the step structure of the Hxc potential by a decomposition of the interaction into basic components. This decomposition allows to write the Hxc potential of the system as a sum over basic Hxc potentials, which can be parametrized in a straightforward manner. Importantly, the decomposition into basic potentials can be generalized to multi-orbital

systems with more than two orbitals. DFT calculations employing the thus parametrized Hxc potentials for double, triple and quadruple quantum dots show excellent agreement with exact results at low temperatures. At higher temperatures, we find moderate quantitative deviations from the exact results that we attribute to the modulation of step widths for finite $\delta n = n_1 - n_2$ not captured in our parametrization. Possible applications of the parametrization of the Hxc potential derived here are the description of transport through multi-orbital quantum dots or molecules coupled to leads. Due to the similarity between broadening by finite temperature on the one hand and finite coupling to the leads on the other hand, we expect that the Hxc potentials for finite coupling to the leads have a similar structure to the ones discussed here.⁵³ One way to incorporate finite coupling to the leads in the Hxc potential is by introduction of an effective temperature.⁵⁴ For the description of non-equilibrium effects the i-DFT framework may be employed which in addition to the Hxc gate potential requires a parametrization of the xc bias.⁵⁵ This would also allow to compute many-body spectral functions of interacting multi-orbital systems.⁵⁶

ACKNOWLEDGMENTS

We acknowledge funding by the grant Grupos Consolidados UPV/EHU del Gobierno Vasco (IT1249-19) as well as the grant of the Ministerio de Economía, Industria y Competitividad, Gobierno de España (MINECO) - Agencia Estatal de Investigación (FIS2016-79464-P) and European Regional Development Fund (FEDER), European Union.

-
- * david.jacob@ehu.es
- ¹ P. Hohenberg and W. Kohn, Phys. Rev. **136**, B864 (1964).
 - ² W. Kohn and L. J. Sham, Phys. Rev. **140**, A1133 (1965).
 - ³ R. M. Dreizler and E. K. U. Gross, *Density Functional Theory* (Springer, Berlin, 1990).
 - ⁴ J.P. Perdew, Phys. Rev. Lett. **55**, 1665 (1985).
 - ⁵ A.D. Becke, Phys. Rev. A **38**, 3098 (1988).
 - ⁶ J.P. Perdew, K. Burke, and M. Ernzerhof, Phys. Rev. Lett. **77**, 3865 (1996); *ibid.* **78**, 1396 (1997)(E).
 - ⁷ J. P. Perdew, A. Ruzsinszky, G. I. Csonka, O. A. Vydrov, G. E. Scuseria, L. A. Constantin, X. Zhou, and K. Burke, Phys. Rev. Lett. **100**, 136406 (2008).
 - ⁸ A.D. Becke, J. Chem. Phys. **98**, 5648 (1993).
 - ⁹ J. Heyd, G. Scuseria, and M. Ernzerhof, J. Chem. Phys. **118**, 8207 (2003).
 - ¹⁰ J. P. Perdew, R. G. Parr, M. Levy, and J. L. Balduz, Phys. Rev. Lett. **49**, 1691 (1982).
 - ¹¹ E. Sagvolden and J. P. Perdew, Phys. Rev. A **77**, 012517 (2008).
 - ¹² P. Gori-Giorgi and A. Savin, Int. J. Quantum Chem. **109**, 2410 (2009).
 - ¹³ P. W. Anderson, Phys. Rev. **124**, 41 (1961).
 - ¹⁴ J. Hubbard, Proc. R. Soc. Lond. A **276**, 238 (1963).
 - ¹⁵ A. Georges, G. Kotliar, W. Krauth, and M. J. Rozenberg, Rev. Mod. Phys. **68**, 13 (1996).
 - ¹⁶ G. Kotliar, S. Y. Savrasov, K. Haule, V. S. Oudovenko, O. Parcollet, and C. A. Marianetti, Rev. Mod. Phys. **78**, 865 (2006).
 - ¹⁷ D. Jacob, K. Haule, and G. Kotliar, Phys. Rev. B **82**, 195115 (2010).
 - ¹⁸ C. Weber, D. J. Cole, D. D. O'Regan, and M. C. Payne, Proc. Nat. Acad. Sci. **111**, 5790 (2014).
 - ¹⁹ M. Karolak, G. Ulm, T. O. Wehling, V. Mazurenko, A. Poteryaev, and A. Lichtenstein, J. Electron Spectrosc. Relat. Phenom. **181**, 11 (2010).
 - ²⁰ R. Requist and E. K. U. Gross, Phys. Rev. B **99**, 125114 (2019).
 - ²¹ J. P. Coe, Phys. Rev. B **99**, 165118 (2019).
 - ²² L. Mazouin, M. Saubanère, and E. Fromager, Phys. Rev. B **100**, 195104 (2019).
 - ²³ K. Haule, Phys. Rev. Lett. **115**, 196403 (2015).
 - ²⁴ O. Gunnarsson and K. Schönhammer, Phys. Rev. Lett. **56**, 1968 (1986).
 - ²⁵ K. Schönhammer, O. Gunnarsson, and R. M. Noack, Phys. Rev. B **52**, 2504 (1995).

- ²⁶ N. A. Lima, L. N. Oliveira, and K. Capelle, *Europhys. Lett.* **60**, 601 (2002).
- ²⁷ N. A. Lima, M. F. Silva, L. N. Oliveira, and K. Capelle, *Phys. Rev. Lett.* **90**, 146402 (2003).
- ²⁸ R. López-Sandoval and G. M. Pastor, *Phys. Rev. B* **67**, 035115 (2003).
- ²⁹ G. Xianlong, M. Polini, B. Tanatar, and M. P. Tosi, *Phys. Rev. B* **73**, 161103(R) (2006).
- ³⁰ K. Capelle and V. L. Campo Jr., *Phys. Rep.* **528**, 91 (2013).
- ³¹ V. Brosco, Z.-J. Ying, and J. Lorenzana, *Sci. Rep.* **3**, 2172 (2013).
- ³² Z.-J. Ying, V. Brosco, and J. Lorenzana, *Phys. Rev. B* **89**, 205130 (2014).
- ³³ D. Carrascal, J. Ferrer, J. Smith, and K. Burke, *J. Phys.: Condens. Matter* **29**, 019501 (2015).
- ³⁴ T. Müller, W. Töws, and G. M. Pastor, *Computation* **7**, 66 (2019).
- ³⁵ C. Verdozzi, G. Stefanucci, and C.-O. Almbladh, *Phys. Rev. Lett.* **97**, 046603 (2006).
- ³⁶ C. Verdozzi, *Phys. Rev. Lett.* **101**, 166401 (2008).
- ³⁷ S. Kurth, G. Stefanucci, E. Khosravi, C. Verdozzi, and E. K. U. Gross, *Phys. Rev. Lett.* **104**, 236801 (2010).
- ³⁸ J. I. Fuks and N. T. Maitra, *Phys. Rev. A* **89**, 062502 (2014).
- ³⁹ J. I. Fuks and N. T. Maitra, *Phys. Chem. Chem. Phys.* **16**, 14504 (2014).
- ⁴⁰ N. Dittmann, J. Splettstoesser, and N. Helbig, *Phys. Rev. Lett.* **120**, 157701 (2018).
- ⁴¹ N. Dittmann, N. Helbig, and D. M. Kennes, *Phys. Rev. B* **99**, 075417 (2019).
- ⁴² G. Stefanucci and S. Kurth, *Phys. Rev. Lett.* **107**, 216401 (2011).
- ⁴³ J. P. Bergfield, Z.-F. Liu, K. Burke, and C. A. Stafford, *Phys. Rev. Lett.* **108**, 066801 (2012).
- ⁴⁴ P. Tröster, P. Schmitteckert, and F. Evers, *Phys. Rev. B* **85**, 115409 (2012).
- ⁴⁵ N. Mermin, *Phys. Rev.* **137**, A1441 (1965).
- ⁴⁶ G. Stefanucci and S. Kurth, *Phys. Stat. Sol. (b)* **250**, 2378 (2013).
- ⁴⁷ S. Kurth and G. Stefanucci, *J. Phys.: Condens. Matter* **29**, 413002 (2017).
- ⁴⁸ T. Dimitrov, H. Appel, J. Fuks, and A. Rubio, *New J. Phys.* **18**, 083004 (2016).
- ⁴⁹ E. Perfetto and G. Stefanucci, *Phys. Rev. B* **86**, 081409(R) (2012).
- ⁵⁰ G. Xianlong, A.-H. Chen, I. V. Tokatly, and S. Kurth, *Phys. Rev. B* **86**, 235139 (2012).
- ⁵¹ P. G. Silvestrov and Y. Imry, *New J. Phys.* **9**, 125 (2007).
- ⁵² Y. Kleeorin and Y. Meir, *Phys. Rev. B* **96**, 045118 (2017).
- ⁵³ S. Kurth and G. Stefanucci, *Phys. Rev. B* **94**, 241103(R) (2016).
- ⁵⁴ N. Sobrino, R. D'Agosta, and S. Kurth, *Phys. Rev. B* **100**, 195142 (2019).
- ⁵⁵ G. Stefanucci and S. Kurth, *Nano Lett.* **15**, 8020 (2015).
- ⁵⁶ D. Jacob and S. Kurth, *Nano Lett.* **18**, 2086 (2018).